ELSEVIER

PII: S0032-3861(97)10105-7

Polymer Vol. 39 No. 18, pp. 4359–4367, 1998

0032-3861/98/$19.00+0.00

Structure development in polyaniline films during electrochemical polymerization. II: Structure and properties of polyaniline films prepared via electrochemical polymerization

Hikaru Okamoto, Masami Okamoto and Tadao Kotaka*
Graduate School of Engineering, Toyota Technological Institute, 2-12-1 Hisakata, Tempaku, Nagoya 468, Japan
(Received 7 August 1997; accepted 8 September 1997)

Structure development in polyaniline (PAn) films was followed during the electrochemical polymerization in 1 M HCl solution via a constant potential mode at $+0.76 \pm 0.03$ V and pH = 0.2 by using several *in situ* and/or *out of situ* techniques including UV-visible spectrometry, chronoamperometry, cyclic voltammetry, Rayleigh scattering and atomic force- and optical microscopy. As the polymerization proceeded from the initial nucleation stage I (where the polymerization current density varies as $I \propto t^0$) to the intermediate stages IIa and IIb ($I \propto t^3 \rightarrow t^2$) and the final stage III ($I \propto t^4$), the gross morphology changed from grainy to fibrillar texture. The fibrils were aggregates of the grains with the size unchanged from that formed in the early stage. This difference between the grainy and fibrillar structures is due to the difference in the state of aggregation of the initially formed grains. In the later stages, however, the fibrils began to form branches, accelerating the rate of polymerization. The branched fibrils grew toward the vertical direction, keeping their horizontal structural size virtually unchanged. © 1998 Elsevier Science Ltd. All rights reserved.

(Keywords: polyaniline; electrochemical polymerization; structural development)

INTRODUCTION

In our preceding paper[1], we examined the electrochemical polymerization behaviour of aniline, using an electrochemical–UV-visible absorption spectrometry (EC–UV) system that enabled us to monitor electrolysis potential, current and UV-visible absorption (UV-Vis) spectra simultaneously as a function of polymerization time. In such a study we confirmed that to obtain films composed of polyaniline (PAn) chains with long average conjugation length and narrow distribution, we should avoid the situation in which pH of the medium becomes high and also the electrolysis potential exceeds +0.8 V. In that context, it is advisable to conduct the polymerization in solutions of low pH around, at most, 0.2 and under a constant potential mode with the applied potential below +0.8 V.

In the electrochemical polymerization of aniline, nucleation and growth first take place on the fresh surface of the electrode. Once the electrode is covered with PAn chains, the deposited chains then play a role of newly formed surface for the subsequent deposition. Thus, not only the primary structure of the deposited PAn chains but also the gross morphology of the film, that govern the acid dissociation constant (pK_a) and conductivity, may dominate the subsequent reaction. It is, therefore, indispensable to examine, during the whole course of the polymerization, the features of structural development, including the primary structure, as well as the gross morphology of the deposited film.

Although there are a number of methods available for observing the fine structure of polymeric materials[2,3], the methods applicable to the observation of structure development during an electrochemical polymerization process are rather limited. In order to monitor structural development, especially the change in the gross morphology during the polymerization process, we also incorporated a time-resolved low-angle laser-light scattering (LLS) photometry into our electrolysis (EC–UV) cell system, in addition to the already installed monitoring systems such as UV-visible spectrometry (UV-Vis), chronoamperometry/potentiometry (CA/CP) and cyclic voltammetry (CV) as described in the preceding paper[1]. Observation of the gross morphology of deposited PAn films was also conducted by atomic force microscopy (AFM) and conventional optical microscopy. Atomic force microscopy (AFM) or scanning tunneling microscopy (STM) is one of the highly potential techniques for observing surface morphology in the real space of varieties of materials including polymers. In fact, morphological studies with AFM were recently applied to some conducting polymers[4–6], and this method was proven to give new information on the fine structure which could never be observed by any other methods. As this technique can be applied to the samples even in solution[7–9], we applied this method to *in situ* and/or *out of situ* observation of nano-size morphology of the PAn films formed via electrochemical polymerization.

In this article we describe our attempts to observe the structural development in PAn films during the whole course of an electrochemical polymerization. Electrolysis was conducted at pH = 0.2 via a constant potential mode at a potential of *ca.* $+0.76 \pm 0.03$ V under which undesirable deterioration of the films[1] was avoided.

* To whom correspondence should be addressed

EXPERIMENTAL

Materials and polymerization method

According to the conclusions of our previous paper[1], we carried out preparation of polyaniline (PAn) films via electrochemical polymerization under a constant potential mode, maintaining the electrolysis potential between + 0.73 to 0.79 V in a medium with its pH adjusted to 0.2. All the measurements were made at 25°C. A typical recipe of the polymerization mixture was 0.1 M (mol/l) aniline in 1 M HCl aqueous solution. Details of the EC–UV polymerization cell system and the method of polymerization were described in the previous paper[1] so that we will not recount them here.

Observation of structure development

Atomic force microscopy (AFM). For the atomic force microscopy (AFM), we employed an AFM (Model SPI 3800, Seiko Instrument Inc., Tokyo). To conduct *in situ* AFM observations, we designed a special Teflon®, cell such as shown in *Figure 1*. The EC–AFM cell was equipped with an indium–tin oxide (ITO) glass electrode (WE), a platinum wire counter electrode (CE) and an AgCl-coated Ag wire reference electrode (RE). The RE was calibrated against a standard Ag/Ag^+/saturated KCl electrode.

For the observation of an early stage of polymerization including nucleation and growth processes, a potential of around + 0.75 V was applied to the ITO electrode (WE) on which PAn chains were deposited. The surface of the deposited PAn film was traced with an Si_3N_4 micro-cantilever coated with gold (the spring constant $C = 0.02$ N/m). However, contact of the cantilever to WE often disturbed the homogeneity of the electrolysis current near the electrode surface, we intermittently stopped the electrolysis, conducted AFM scan usually within 10 min, separated the cantilever sufficiently from the electrodes so that the current was not disturbed and then resumed electrolysis.

On another occasions, *out of situ* AFM observation with a dynamic (tapping) mode was conducted on resulting PAn films in an ambient atmosphere. We took out WE with deposited PAn film from the cell and rinsed it well in pure water and dried it in vacuum at room temperature for more than one day to subject it to AFM observation. We used an Si micro-cantilever of the spring constant $C = 17$ N/m and the resonance frequency $f = 138$ kHz. PAn films deposited in a large amount often spontaneously peeled off from WE during the rinsing process. Then we scooped fragments onto a mica sheet and subjected it to AFM observation.

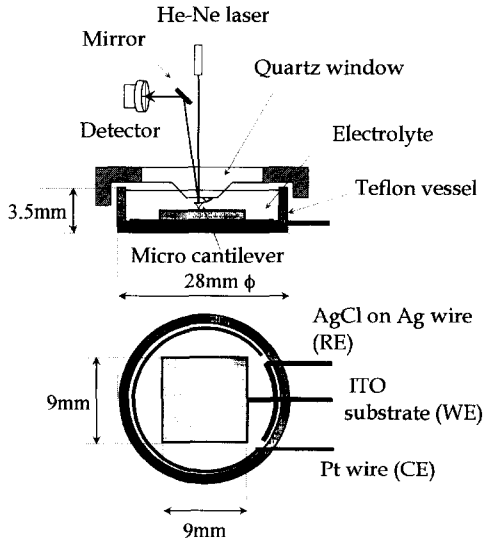

Figure 1 Configuration of the electrochemical–atomic force microscopy (EC–AFM) cell assembly

Time-resolved Rayleigh scattering photometry. For *in situ* observation of the gross morphology development, we employed a time-resolved Rayleigh scattering photometry. To this end we also designed a special electrolysis–light scattering (EC–LS) cell such as shown in *Figure 2b* and mounted on a multi-purpose home-made low-angle laser light scattering (LLS) system shown in *Figure 2a* (H. Sato, M. Okamoto and T. Kotaka, unpublished).

The EC–LS cell consisted of an ITO glass electrode used as a working electrode (WE), a Pt wire counter electrode (CE) and an AgCl-coated Ag wire reference electrode (RE). A transparent polyvinyl-chloride film was used as an upper window and the ITO glass electrode (WE) itself as a lower window, maintained at 9 mm separation.

The incident light was a plane polarized light from a 15 mW He–Ne laser source incident on the cell through WE and the scattered light intensities were detected with a 38-channel photodiode array (PDA: S4111-38Q; Hamamatsu Photonics) mounted on an XY stage held with a vertical guide rail. During a test run, we placed an analyzer between the cell and PDA and confirmed that the Hv component gave out no signals so that PAn chains were, in effect, isotropic in the plane of the electrode and grown perpendicular to the electrode surface (cf., *Figure 8*). Whenever necessary, the scattering pattern was recorded on a Polaroid camera of the shutter speed adjustable between 1/2 to 1/500 s. By sliding the PDA position vertically along the guide rail, we detected scattered light intensities covering the angle θ between (a) 1.84 and 8.58° ($q^{-1} = 500$–2340 nm); and between (b) 6.24 and 27.2° ($q^{-1} = 160$–690 nm).

Rayleigh scattering data were analyzed in the usual way[10]. The scattering intensity, $I_s(q)$, at an angle θ is expressed as a function of the scattering vector, q, defined by:

$$q = (4\pi n/\lambda_0) \sin(\theta/2), \tag{1}$$

where n is the refractive index of the medium surrounding the particles and λ_0 the wavelength *in vacuo* of the incident light. q^{-1} represents the length scale of the scattering particles. The angular dependence of the scattered light intensity, $I_s(q)$, is given as:

$$I_s(q) = I_0 K' N M^2 P(q, m, r) S(q) \tag{2}$$

and the invariant Q proportional to the volume fraction of the scattering particles as:

$$Q = \int q^2 I_s(q) dq \tag{3}$$

where I_0 is the incident light intensity, K' is an experimental constant, N is the number of scattering particles in unit volume, and M is the particle mass. The parameter r is related to the size of the scattering particle and m is the relative refractive index of the particle to the medium. The intra-particle scattering factor $P(q, m, r)$ contains information on the average particle size, shape and internal structure, while the inter-particle scattering factor $S(q)$ represents the interference of the light scattered from different particles. In a well ordered array of the particles, $S(q)$ leads to a regular diffraction pattern.

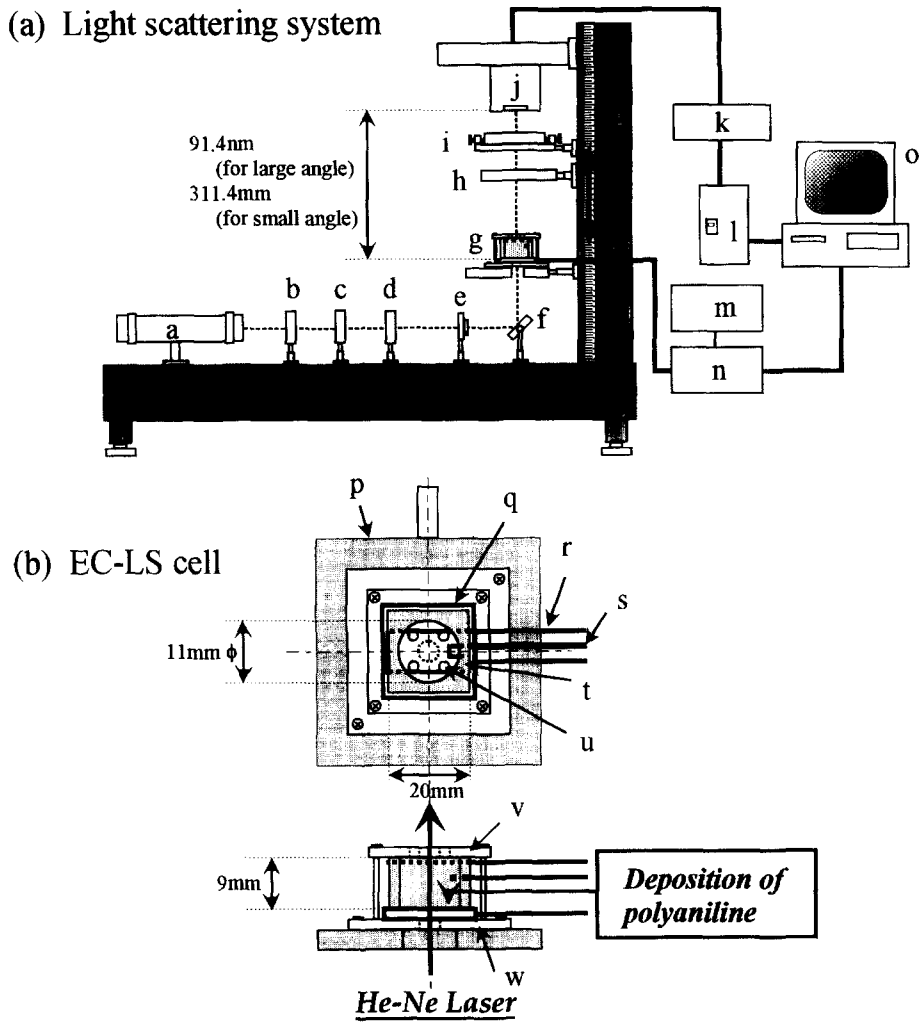

Figure 2 Configuration of (a) the multipurpose light scattering (LLS) system utilized for monitoring the electrochemical polymerization process; and (b) that of the electrochemical–light scattering (EC–LS) cell assembly. The LLS system consists of a: He–Ne laser; b: shutter; c: polarizer; d: ND filter; e: pinhole; f: mirror; g: EC–LS cell; h: analyzer; i: Polaroid camera; j: photodiode array (PDA); k: A/D converter; l: power source; m: function generator; n: potentiogalvanostat; o: data processor; whereas the EC–LS cell consists of p: sample stage; q: ITO glass working electrode (WE); r: Pt wire counter electrode (CE); s: AgCl on Ag-wire reference electrode (RE); t: silicone rubber bulk head; u: gas outlet; v: upper transparent window; w: lower fixer

Optical microscopy (OM). Next, in order to observe macro-size structure or the gross morphology development, we also conducted optical microscopic (OM) observation, using a cell of the configuration similar to the EC–LS cell, but of a much smaller size. The polymerization was carried out on a sample stage of an optical microscope of the maximum 100 × magnification (OPTIPHOT2-POL; Nikon Co, Tokyo). The pictures were recorded on a digital camera (DC40; Kodak) for convenience of later data processing.

RESULTS

UV-visible chronoabsorptiometry and chronoamperometry

Figure 3 shows a series of UV-Vis spectra collected at 2-min intervals from the beginning of the polymerization up to 24 min. We see that the spectra obtained at different times are nearly identical in shape and develop with time, maintaining the peak position at a constant wavelength of around 750 nm. This is in contrast to the case of a constant current mode electrolysis reported in Part 1, in which the peak shifted gradually to the longer wavelength side and the spectrum also changes its shape, reflecting the slight decrease in polymerization potential (cf., *Figure 2a* in Ref. 1). Thus, in the constant potential mode polymerization the absorption peak strength at 750 nm could be a good measure to monitor the amount of PAn chains produced. However, the peak strength increases rather rapidly with time and exceeds the upper limit of the experimental window of the UV-Vis spectrometer (optical density of *ca.* 2). Thus, the absorption peak strength at 750 nm can no

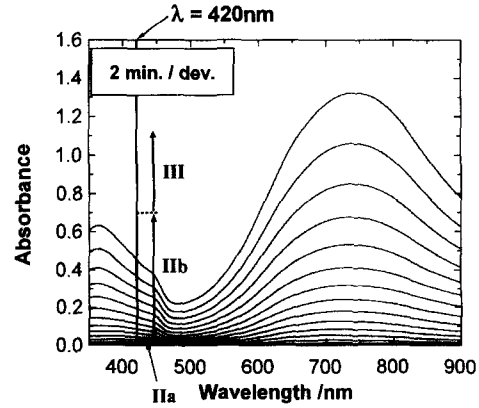

Figure 3 Development of UV-visible spectra monitored at 2-min intervals during the electrochemical polymerization at + 0.75 V. For the zones marked as IIa, IIb and III see *Figure 4*

longer directly reflect the amount of PAn chains at high yields. To make further observation possible, we selected the absorption strength at 420 nm for observation, which was attributed to the peak wavelength of radical cation (polaron) species[11] and favorably used by many researchers[12–14]. Thus, we also monitored development of the absorption strength at 420 nm under four different potentials within + 0.73 and + 0.79 V. We also monitored electrolysis current density I, which is supposed to be proportional to the polymerization rate at the particular instant.

Figure 4 shows double logarithmic plots of developments of (a) absorption strength at 420 nm; (b) electrolysis current density I; and (c) total amount of consumed coulombs (which is the integral of the current *versus* time curve) with polymerization time t. In *Figure 4b*, we see that the current density I remains constant for the first few hundred seconds, and then starts increasing rapidly with time in such a way that $I \propto t^3$, then $I \propto t^2$ and still later $I \propto t^4$. This tendency seems to be common for the polymerization at different potentials, as long as they were maintained within + 0.73 to 0.79 V. We thus separated the time span into four regions I, IIa, IIb, and III, where $I \propto t^0$, $I \propto t^3$, $I \propto t^2$ and $I \propto t^4$, respectively, as seen in *Figure 4* for the polymerization profile (filled symbols) at + 0.75 V. The region boundaries at lower potential shift to the longer time side and those at higher potentials to the shorter time side, as anticipated.

The time development profiles of the absorbance and consumed coulombs shown in *Figure 4a* and *c*, respectively, reflect the amount of PAn chains deposited, and match rather neatly with each other, although the distinction between the four different regions is not quite clear, as in the case of the current density profiles. The comparison of these profiles should tell us the efficiency of polymerization, if the specific absorbance of the growing PAn chains were known, which is not yet the case. In any case, these time development profiles should reflect differences in the polymerization mechanisms in these four different regions, which we will discuss later. We also conducted direct observation of the gross morphology of deposited PAn films at the different stages marked as A, B, C, etcetera up to H. Again this will be discussed later.

In stages II–III, rapid increase in the current density with time implies that the deposition rate is accelerated as the polymerization proceeds. In other words, deposited PAn chains exert an autocatalytic activity[15,16] towards the further deposition of aniline on the PAn film. To confirm if such an autocatalytic effect were true or not, we repeated cyclic voltammetry (CV) several times by sweeping the potential at a rate of 10 mV/s first from − 0.2 V (the reduction level) to + 1.1 V (the over-oxidation level, which was above the critical potential of + 0.8 V)[1] and back to − 0.2 V, and for the second run from − 0.2 to + 1.0 V and back, and finally up to + 0.8 V, as indicated in *Figure 5*, in which the CV patterns obtained are summarized.

In the first scan, the current begins to increase, indicating onset of the polymerization on the WE surface when the potential exceeds + 1.0 V, obviously because the initiation or nucleation is driven by the over-potential. As the CV scan is repeated, the potential at which the current begins to increase shifts to the lower potential side, indicating that the polymerization can now proceed at this lower potential,

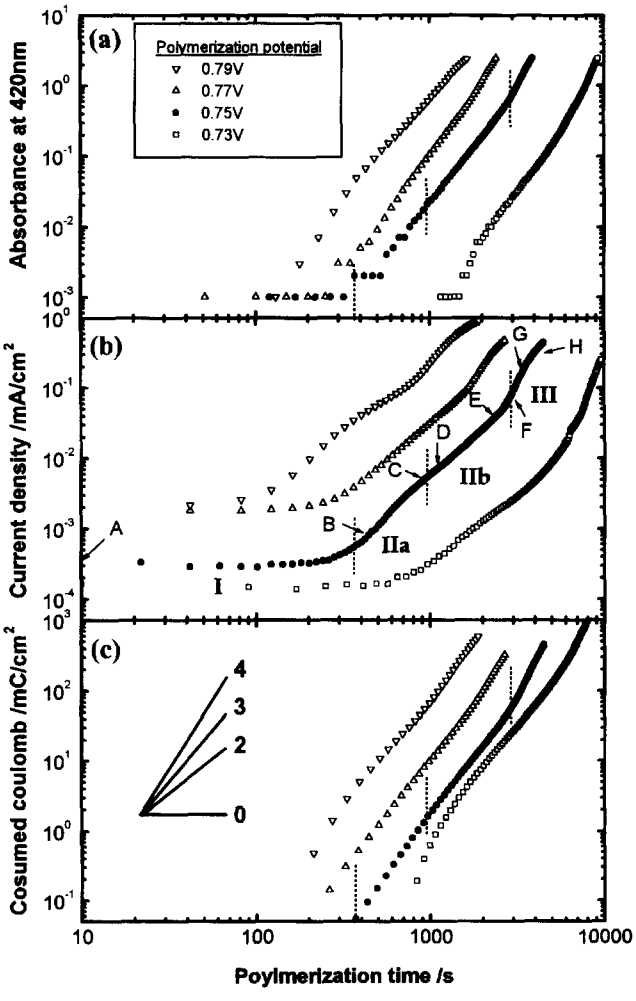

Figure 4 Double logarithmic plots for the development of (a) absorbance at 420 nm light; (b) electrolysis current density; and (c) consumed coulombs during the electrochemical polymerization of 0.1 M aniline in 1 M HCl solution under four different potentials between + 0.79 to 0.73 V. The marks A, B, C, etcetera up to H indicate the PAn films subjected to the direct observation via AFM and OM of the gross morphology shown later in *Figure 6*

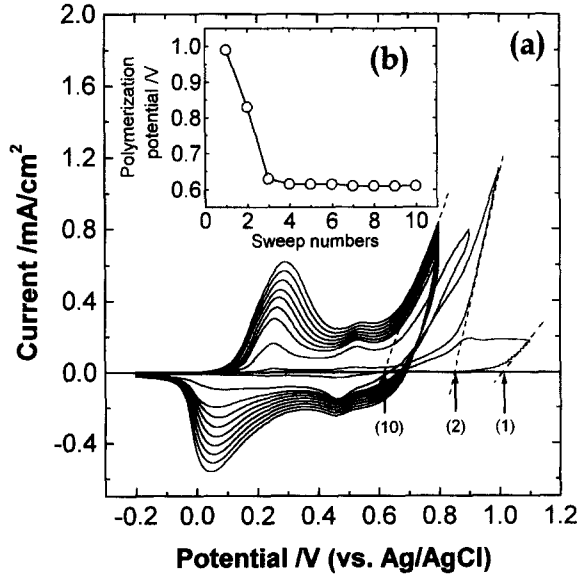

Figure 5 (a) Cyclic voltammograms of PAn film in the early stages of polymerization; and (b) change of the polymerization potential with the sweep numbers. The cyclic voltammetry was repeated ten times by sweeping the potential at a rate of 10 mV/s first from − 0.2 V to + 1.1 and back to − 0.2 V, and for the second run from − 0.2 V to + 1.0 V and back, and finally up to + 0.8 V

which we may tentatively call polymerization potential. In the insert of *Figure 5* showing a plot of the polymerization potential *versus* scan number, we see that the potential gradually decreases from +1.0 V for the fresh ITO surface and levels off at about +0.6 V after repeating the cycle three times. These results are an indication of the autocatalytic action of the deposited PAn chains, which obviously reduce the polymerization potential below the level of the fresh WE surface. Subsequent growth occurs around these nuclei created in the early stage of polymerization.

Direct observation of gross morphology

In situ *AFM observation.* In order to make clear what happened in each region of stages 'I, IIa, IIb and III', we directly observed structural development at the points marked as A, B, C, etcetera up to H in *Figure 4*, using AFM and OM methods.

Figure 6a shows *in situ* AFM images of PAn chains at points A–D from 10 to 1000 s. These images show that semispherical aggregates of PAn chains first appear on the surface and then grow upwards.

Unfortunately we could not make *in situ* observations after 1000 s, because the cantilever suffered unusual forces on approaching the electrode densely covered with growing PAn chains, as if a diver were trapped in a jungle of seaweed. In order to observe the gross morphology of the growing PAn chains in the intermediate to late stages IIb to III corresponding roughly to 2000–5000 s polymerization time, we carried out an OM observation of PAn chains polymerized on a sample stage of an optical microscope. *Figure 6b* shows the images at points E–H in *Figure 4*. At stage E, the electrode surface showed a greenish color, but any structure was not seen at the 100 × magnification. As electrolysis proceeded to stages G–H in region III, we could barely observe aggregated fibrillar structures. As the polymerization further proceeded, the color of the film became deeper, keeping the aggregated fibrillar structure unchanged.

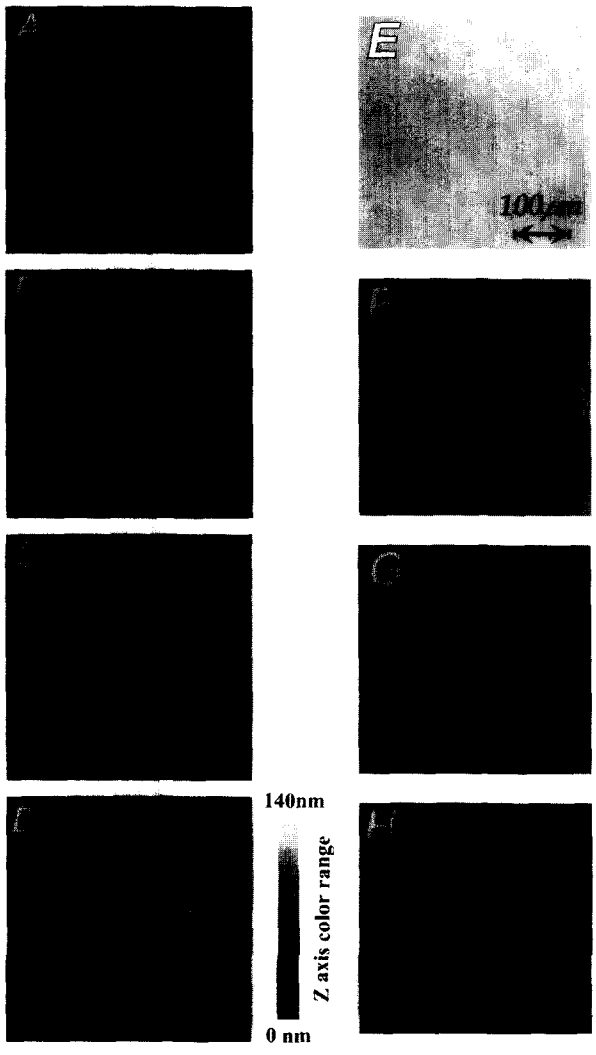

Figure 6 *In situ* observations of PAn film developed by electropolymerization by electrochemical (a) atomic force; and (b) optical microscopy. Marks A, B, C etc show the points of data collection shown in *Figure 4b*

Out of situ AFM observation. After *ca.* 1000 s polymerization, the deposited film became soft and jelly-like, preventing further *in situ* AFM observation. We thus made *out of situ* AFM observation on such a film, although, as already mentioned, a part of the deposited PAn film often spontaneously stripped off from the electrode during the rinsing process in water. In such a case, we scooped up fragments onto a mica substrate and compared the morphology with that still stuck to the electrode.

Figure 7 shows AFM images of PAn film on ITO taken in the final stage H at three different magnifications, as indicated. The morphology of the stripped fragments corresponds to needle-like or fibrillar aggregates observed in the intermediate stage IIb (G–H) of *in situ* optical microscopy. At high magnifications, we notice that fibrils consist of aggregates of PAn grains of ~60 nm diameter and their sizes are almost the same. This result suggests that the grains aggregate into fibrils, which in turn develop into an entanglement network with branching and cross-linking, as the polymerization further proceeds. The structural sizes of the grains and fibrils are only slightly dependent on the polymerization potential. A lower potential leads to the structure with a slightly larger size.

In situ *Rayleigh scattering.* Rayleigh scattering photometry is expected to reveal the structural features of a few tens to hundred nm scale, which is obviously larger than the scales observable by AFM. On the other hand, the scattered light intensity $I_s(q)$ is proportional to the square of the mass of the scattering particles, as seen in equation (2), which implies that the light scattering photometry is effective in collecting the structural information on the late stage III electrochemical polymerization.

Another crucial issue in the LS analysis of PAn films is the fact that PAn chains are known to assume a greenish oxidized (emeraldine) form under the polymerization potential of +0.75 V and only at −0.2 V become a colorless reduced (leucoemeraldine) form. The PAn film deposited at +0.75 V thus absorbed scattered light, making *in situ* LS measurements virtually impossible. To circumvent this difficulty, we switched the potential from +0.75 to −0.2 V, at which the polymerization temporarily stopped and the deposited PAn film was gradually reduced to a colorless form and the scattering pattern became observable. After collecting scattering data, the potential was switched back to +0.75 V where polymerization resumed. *Figure 8* shows (a) spectra taken at +0.75 and −0.2 V in the late stage III of polymerization; and (b) the corresponding Rayleigh scattering patterns recorded on Polaroid film. Interestingly, the pattern at −0.20 V looks as if the scattering particles are arranged on a regular two-dimensional array.

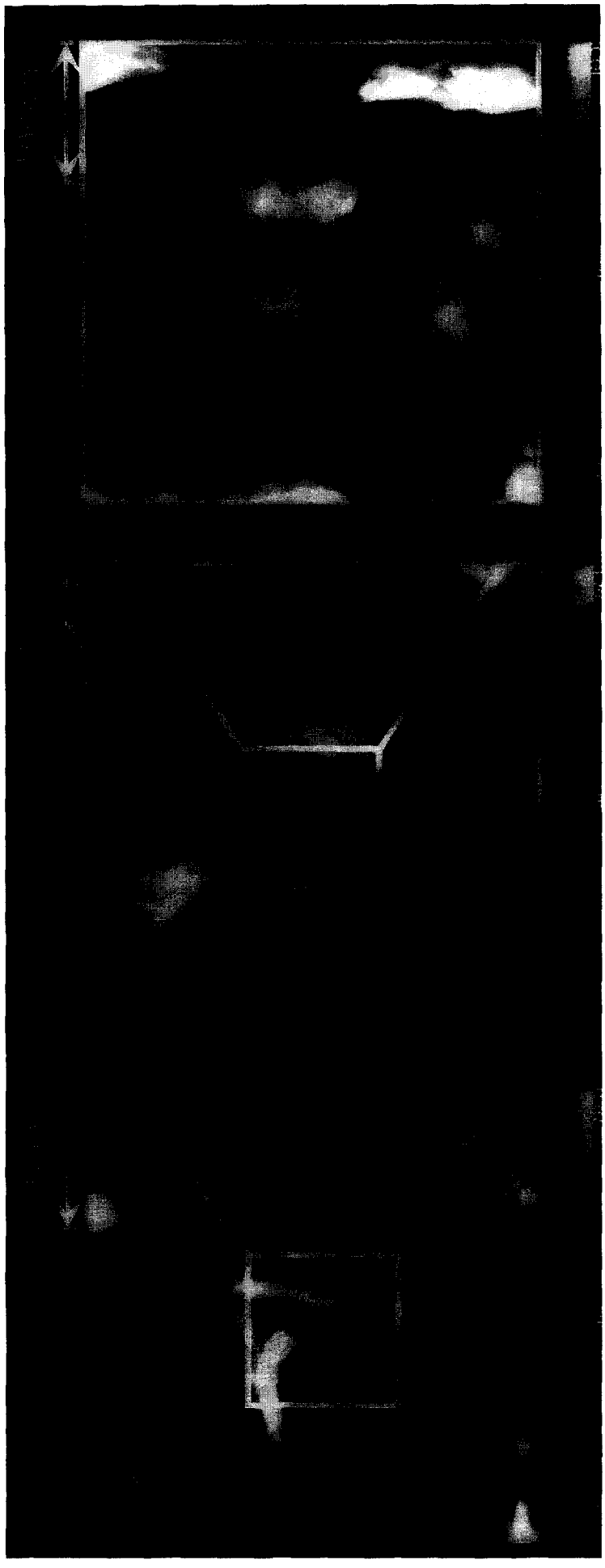

Figure 7 *Out of situ* AFM images taken in the final stage H at three different magnifications

In conducting the '*in situ*' scattering observation, we employed this potential switching technique: the system was alternatively maintained at an oxidation potential of + 0.75 V for 60 s for polymerization to proceed and then switched to the reduction potential of − 0.2 V for 180 s for LS observation. Examining closely the current density profile *versus* polymerization time t shown in *Figure 9a* we noticed that on switching up to the polymerization potential the current reached the steady state relatively rapidly, but on switching down to the reduction potential the current reached the steady state slowly. In fact, when the potential was switched from the reduction (− 0.2 V) to oxidation potential (+ 0.75 V), the current once increased sharply, owing presumably to the charging up of the electric double layer and/or the doping of Cl^- ion into the deposited PAn film and then decreased to reach the steady-state polymerization current. When the potential was reversed from + 0.75 to − 0.2 V, the current once hit a negative peak and resumed almost instantly a zero value, reflecting the fact that the discharging of the double layer and/or the dedoping of the PAn film are a rapid process.

As a consequence, it was necessary to wait for some time for the color of the oxidized solution to fade away. Then we collected LS data during the last 5 s of the 180 s reduction period just before resuming the oxidation potential. *Figure 9b* shows development of the change in current density during such potential-switching cycles plotted in double logarithmic scale and *Figure 9c* that of the LS invariant Q (in arbitrary scale). In these plots we assumed that the effective polymerization time is one-quarter of the net time elapsed. In *Figure 9b* the current density profiles for the reduction phase are omitted because they go to negative values. The envelop corresponds to the current density change at the polymerization potential which can be divided into the four stages of I, IIa, IIb and III.

In *Figure 9c* we see that the LS invariant Q is virtually invisible in the early to intermediate stages I and II, but in stage III it develops very rapidly with time as $I_s(q) \propto t^8$, corresponding to the late stage of polymerization where the current density is $I \propto t^4$.

Figure 10 shows three-dimensional plots (all in linear scale) of the q-dependence of scattering intensities $I_s(q)$ *versus* polymerization time t (a) for large angles of q^{-1} = 160–690 nm; and (b) for the small angles of q^{-1} = 500–2340 nm. The scattering profiles are surprisingly unique: in the early stages before 2000 s, we see virtually no signals. In late stage III, however, the peaks begin to develop, in which we see the intensity at each peak increases with time t very rapidly as $I_s(q) \propto t^8$ without changing its location in the q space.

DISCUSSION

According to Brett and Brett[17], in a process of electrodeposition such as electroplating, the mechanism involves, as a first step, the deposition of a metal ion on the electrode surface to form an adatom, on which other atoms aggregate forming a nucleus which then grows parallel and/or perpendicular to the electrode surface. Once the surface is covered with at least a monolayer of the metal, the electrochemical properties of the new surface dominate subsequent deposition. Such a situation is more or less similar to that in the electrochemical polymerization of aniline forming a film of PAn chains.

In electrodeposition including electrochemical polymerization, nucleation normally follows a first-order rate process[17] in that the number N of nuclei develops as:

$$N = N_0[1 - \exp(-At)] \quad (4)$$

where N_0 is the number of nucleation sites and A the nucleation-rate constant.

In an extreme case of instantaneous nucleation where $At \gg 1$, $N = N_0$ and in the other extreme of continuous nucleation where $At \ll 1$, $N = AN_0t$[17]. In the subsequent growth phase, growth presumably proceeds on the nuclei with the surface area proportional to r^2, where r is the radius. Then if we introduce a linear dependence of r on t for a kinetically controlled process under instantaneous nucleation, the current density I should be $I \propto r^2 \propto t^2$, whereas under continuous nucleation, $I \propto r^2N_0t \propto t^3$[17]. By looking at the current density *versus* polymerization time data shown in *Figure 4b*, we notice in the early stage of the growth phase IIa $I \propto t^3$, suggesting that the electrochemical polymerization proceeds along more or less the same mechanism as in the early phase of electrodeposition, such as in electroplating.

In *Figure 3* we see the UV-Vis spectra corresponding to the intermediate stages IIa and IIb develop with time in such a way that the shape hardly changes but their intensity increases steadily, almost parallel with the time development of the consumed coulombs, as seen in *Figure 4*. This behaviour suggests that the polymerization of PAn chains proceeds in a nucleation-controlled manner, in that once a nucleus is formed, a chain grows very rapidly until its backbone conjugation length becomes sufficiently long. Subsequently, the number of the chains increases as time goes by. These chains eventually aggregate into grains, which in turn form fibrils, and finally bundles of the fibrils.

Based on these observations together with the scattering patterns shown in *Figure 10*, we propose a model for

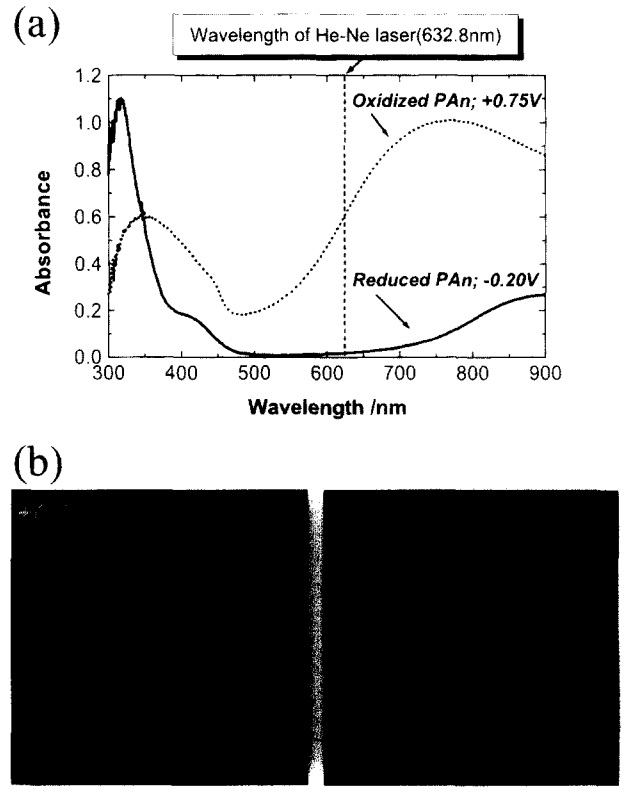

Figure 8 (a) UV-Vis absorption spectra; and (b) light scattering patterns of PAn film under polarization at + 0.75 and − 0.20 V

electrochemical polymerization of aniline such as that shown in *Figure 11*. In the initial stage I, an overpotential initiates formation of the nuclei and the electrolysis current develops as $I \propto t^0$. This nucleation occurs to yield grainy particles of *ca.* 60 nm diameter on a more or less regular two-dimensional array on the electrode surface, although its exact configuration is not yet clear. Then the intermediate region IIa follows, which is a two-dimensional growth process, and grainy layers are gradually formed. In this region IIa, the nucleation and the following rapid chain growth continuously occur, then $I \propto t^3$. Region IIb is a one-dimensional growth process due presumably due to the structural change from grainy aggregates to fibrils of *ca.* 110 nm diameter and following bundling of such aggregates or fibrils, $I \propto t^2$. The final stage III is the branching, cross-linking and the bundling processes. As the branching/network formation via cross-linking make the reaction surface larger, then it could be that $I \propto t^4$. Since the light scattering intensity is proportional to the square of the mass deposited, $I_s(q) \propto (mass)^2$, and the mass increases as $mass \propto t^4$, then the scattering invariant develops as $Q \propto I_s(q) \propto t^8$. The fibrillar aggregates of the grains and branched and/or cross-linked fibrils further aggregate into bundles, which grow as if bamboo shoots after a rainfall toward the vertical direction, keeping their horizontal structural size of the order of several hundreds of nanometers virtually unchanged, resulting in unique scattering patterns, such as those seen in *Figure 10*.

The proposed model constitutes our tentative conclusion on the mechanisms, processes and structure development during the course of electrochemical polymerization of PAn films.

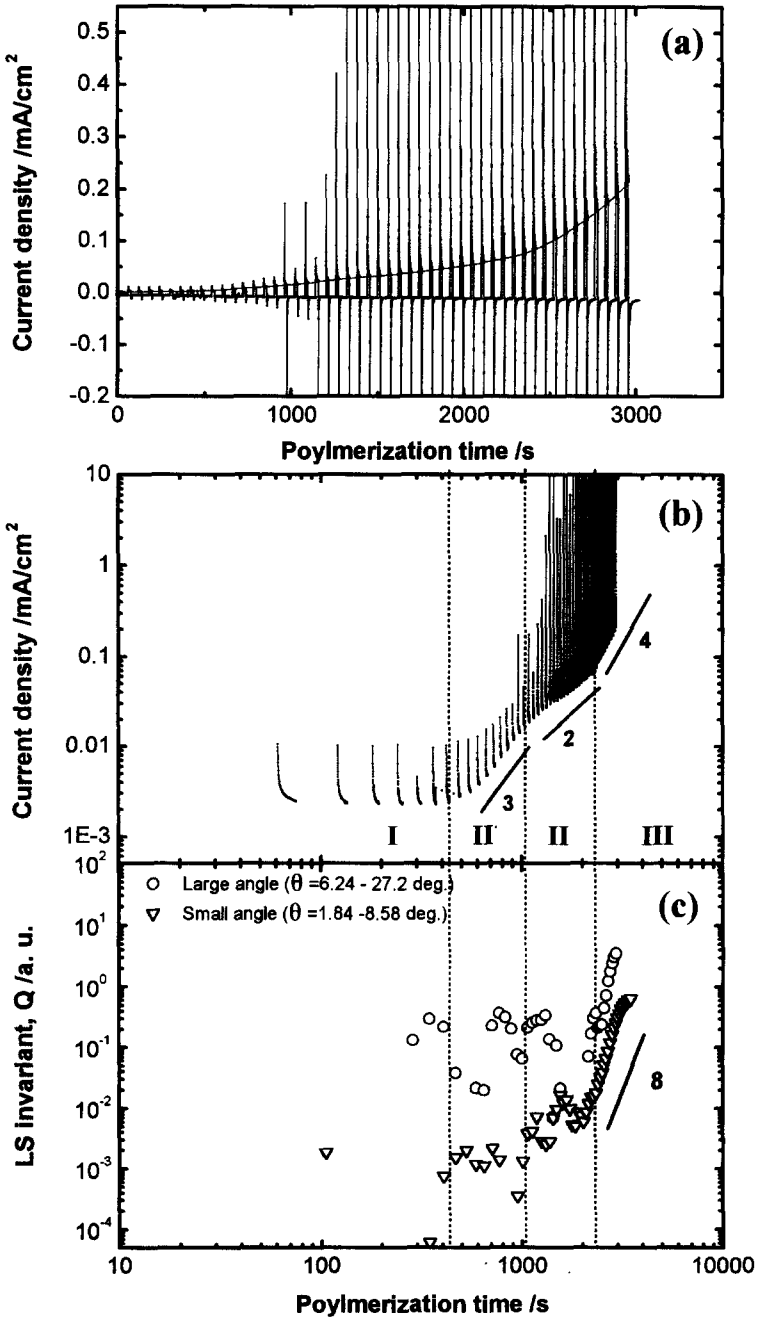

Figure 9 Development of current with polymerization time in (a) linear; and (b) double logarithmic scale; and (c) that of the LS invariant Q

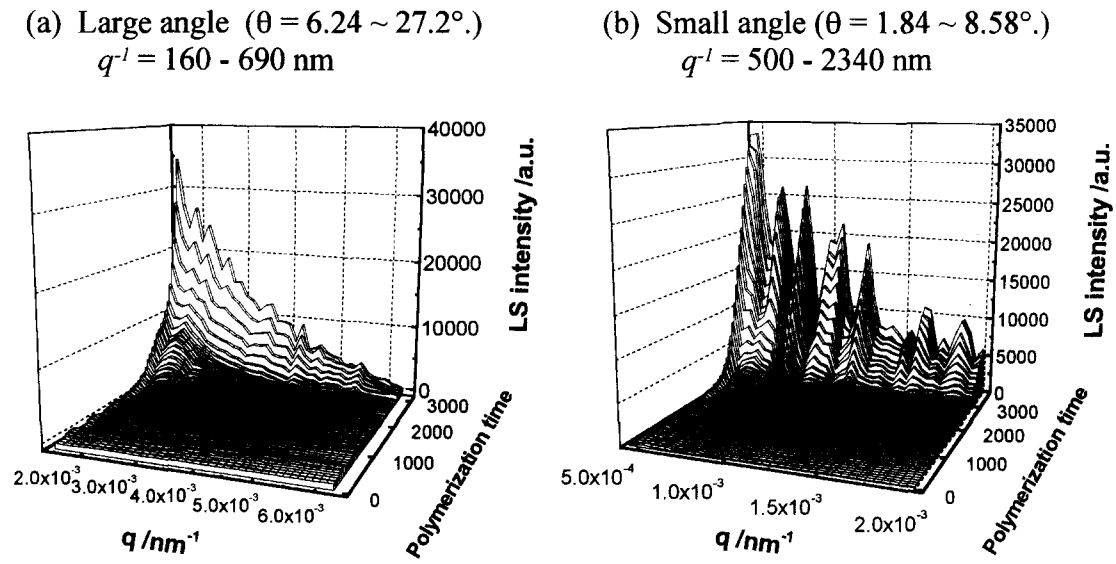

Figure 10 Three-dimensional plots of the q-dependence of scattering intensities $I_s(q)$ *versus* polymerization time t (a) for large angles of q^{-1} = 160–690 nm; and (b) for the small angles of q^{-1} = 500–2340 nm

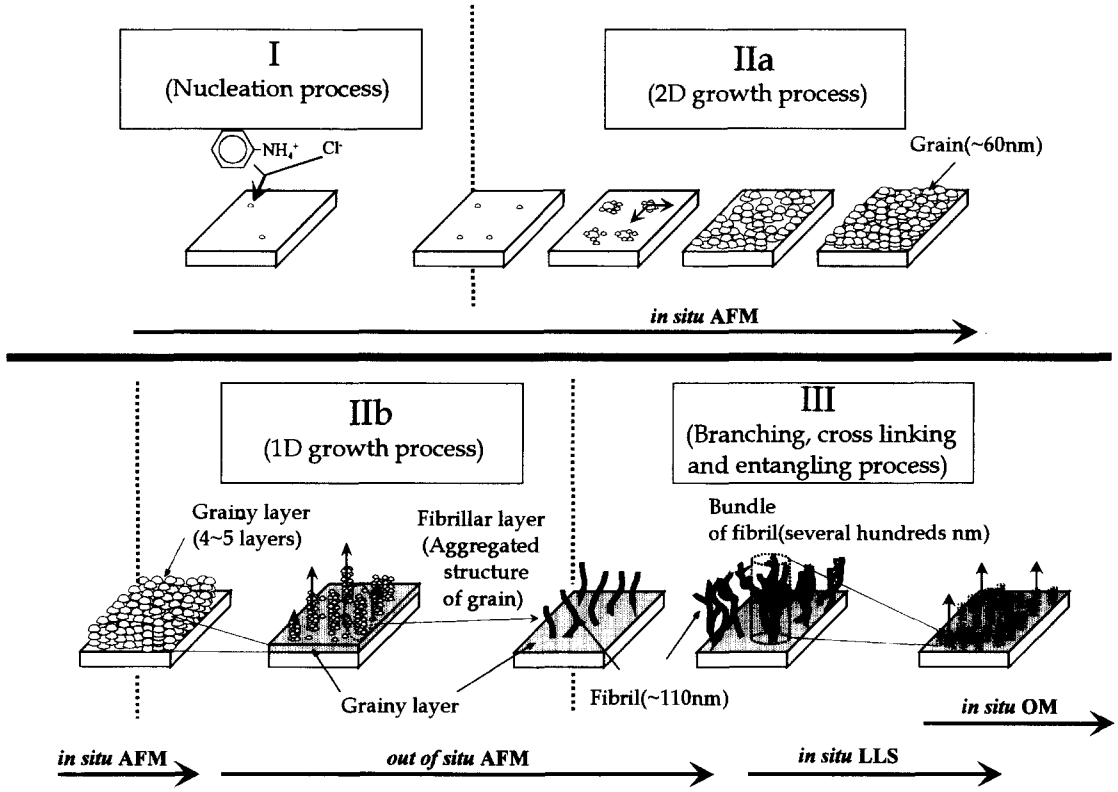

Figure 11 A structure development model for electrochemical polymerization of a PAn film

REFERENCES

1. Okamoto, H. and Kotaka, T., *Polymer*, in press.
2. Campbell, D. and White, J. R., *Polymer Characterization; Physical Techniques*. Chapman and Hall, New York, 1989.
3. The Society of Polymer Science, Japan (eds), *Shin Koubunshi Jikkengaku*, Vol. 5–7. Kyoritu, Tokyo, 1995.
4. Armes, S. P., Aldissi, M., Hawley, M., Beery, J. G. and Gottesfeld, S., *Langmuir*, 1991, **7**, 1447.
5. Jeon, D., Kim, J., Gallagher, M. C. and Willis, R. F., *Science*, 1992, **256**, 1662.
6. Vela, M. E., Zubimendi, J. L., Ocon, P., Herrasti, P., Salvarezza, R. C., Vazquez, L. and Arvia, A. J., *Electrochimica Acta*, 1996, **41**, 1891.
7. Kim, Y. T., Yang, H. and Bard, A. J., *J. Electrochem. Soc.*, 1992, **138**, L71.
8. Li, J., Wang, E., Green, M. and West, P. E., *Synthetic Metals*, 1995, **74**, 127.
9. Avlyanov, J. K., Josefowicz, L. Y. and MacDiarmid, A. G., *Synthetic Metals*, 1995, **73**, 205.
10. Brown, W., *Light Scattering; Principles and Development*. Oxford University Press, New York, 1996, p. 477.
11. Stilwell, D. E. and Su-Moon Park, *J. Electrochem. Soc.*, 1989, **136**, 427.
12. Koziel, K., Lapkowski, M. and Lefrant, S., *Synthetic Metals*, 1995, **69**, 217.
13. Yang, S. C., Cushman, R. J. and Zhang, D., *Synthetic Metals*, 1989, **29**, E401.
14. Yoon-Bo Shim, Mi-Sook Won and Su-Moon Park, *J. Electrochem. Soc.*, 1990, **137**, 538.
15. Noufi, R., Nozik, A. J., White, J. and Warren, L. F., *J. Electrochem. Soc.*, 1982, **129**, 226.
16. Stilwell, D. E. and Park, S. M., *J. Electrochem. Soc.*, 1990, **137**, 538.
17. Brett, C. M. A. and Brett, A. M. O., *Electrochemistry: Principles, Methods and Applications*. Oxford University Press, New York, 1994, p. 341.